ACS OMEGA

Article

Cite This: ACS Omega 2019, 4, 7650−7657

http://pubs.acs.org/journal/acsodf

CZTS Decorated on Graphene Oxide as an Efficient Electrocatalyst for High-Performance Hydrogen Evolution Reaction

Renuka V. Digraskar,[†] Vijay S. Sapner,[†] Shivsharan M. Mali,[†] Shankar S. Narwade,[†] Anil V. Ghule,[‡] and Bhaskar R. Sathe*[,†]

[†]Department of Chemistry, Dr. Babasaheb Ambedkar Marathwada University, Aurangabad 431004, Maharashtra, India

[‡]Department of Chemistry, Shivaji University, Kolhapur 416004, Maharashtra, India

Supporting Information

ABSTRACT: Cu_2ZnSnS_4 (CZTS) was synthesized by the sonochemical method using 2-methoxyethanol as the solvent and subsequently decorated onto graphene oxide (GO synthesized by the modified Hummers' method) using two different approaches such as in situ growth and ex situ synthesis followed by deposition. Preliminary characterizations indicated that the synthesized CZTS belongs to the kesterite structure with a sphere-like morphology. The in situ-synthesized CZTS/GO (I-CZTS/GO) composite is used as an efficient electrocatalyst for hydrogen evolution reaction (HER) which revealed superior electrocatalytic activity with a reduced overpotential (39.3 mV at 2 mA cm^{-2}), Tafel slope (70 mV dec^{-1}), a larger exchange current density of 908 mA cm^{-2}, and charge transfer resistance (5 Ω), significantly different from pure CZTS. Besides, the I-CZTS/GO composite exhibits highest HER performance with high current stability of which shows no noticeable degradation after *i*−*t* amperometry. The catalytic activity demonstrates that the I-CZTS/GO composite could be a promising electrocatalyst in hydrogen production from their cooperative interactions.

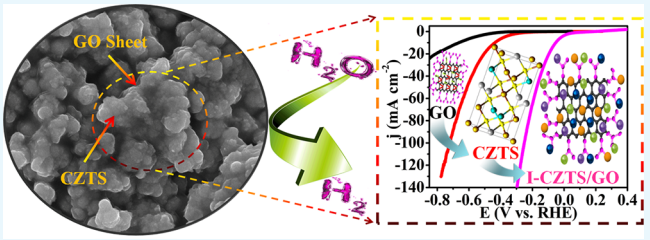

INTRODUCTION

Hydrogen (H_2) is viewed as one of the promising energy carriers, holding marvelous potential for clean and sustainable energy technology.[1] The most common ways for the large-scale production of H_2 includes natural gas reforming and gasification of coal and petroleum coke, which lead to CO_2 emission (greenhouse gas), and also, these processes are not energy-efficient.[2] H_2 production by splitting of water by the electrochemical method has attracted attention of researchers because of having a simple and sustainable way for it.[3] Accordingly, to improve the rate of hydrogen evolution reaction (HER) below the overpotential, Pt and Pt-based systems are commonly used. Unfortunately, their scarcity and high cost hinder their large scale production.[4] Thus, the development of equally efficient, abundant, nontoxic, and nonprecious replacement electrocatalysts has become a main research focus. For example, the most commonly used nonprecious HER catalysts include transition-metal sulfides,[5] phosphides,[6] carbides,[7] nitrides,[8] and noble metal-free alloys.[9] Even though most of the above listed systems usually suffer from poor HER activity and stability, recently, it is well accepted that the surface structure and their electrical conductivity are the two key parameters that alter their HER activity.[10] On the other hand, carbon materials (graphene, carbon nanotube, fullerene C_{60}, etc.) are ideal supports to further tune their activities owing to their extraordinary physicochemical properties.[11] Specifically, graphene, a few layer and two dimensional carbon material, has attracted more attention as the supporting material for HER catalysts.[12] The use of graphene as a support not only improves the conductivity of the hybrid catalysts but also improves the dispersity because of their comparatively huge active surface area. Hence, the graphene-based systems usually show enhanced response toward HER.[13] For example, Niyitanga and Kyung Jeong reported that the MoS_2/graphene oxide (GO) shows enhanced performance toward HER with respect to MoS_2.[14] Yin et al. reported that the activity of Ni−(MoS_2/GO) is better than that of Ni−GO and Ni−MoS_2.[15] Ma et al. also reported that the nanocomposite of CoP nanoparticle reduced GO (rGO) shows HER with a low overpotential and high current density with respect to pure CoP nanoparticles.[10] Ma et al. found the MoS_2NFs/rGO paper serves as a freestanding, flexible, and durable working electrode, having improved activity with respect to individual components toward HER.[16] Recently, transition-metal chalcogenides including MoS_2,[11c,17] WS_2,[18] Ni_3S_2,[4a] $CoNi_2Se_4$,[19] and $NiFeS_2$[14] have justified to be good HER electrocatalytic systems with high activity and low cost. However, the complicated synthetic protocols and harsh conditions of these chalcogenides limit their usage. In this manuscript, two facile approaches (in situ and ex situ) are developed to synthesize the novel CZTS/GO composite by the one-step

Received: December 21, 2018
Accepted: March 6, 2019
Published: April 26, 2019

DOI: 10.1021/acsomega.8b03587
ACS Omega 2019, 4, 7650−7657

sonochemical method. The in situ-synthesized CZTS/GO (I-CZTS/GO) exhibits an enhanced activity toward HER compared to pure CZTS and GO.

RESULTS AND DISCUSSION

As shown in Scheme 1, the pathway for fabrication of the I-CZTS/GO electrocatalytic system represents the metal

Scheme 1. Schematic Illustration of Different Steps for Synthesis of I-CZTS/GO Composites

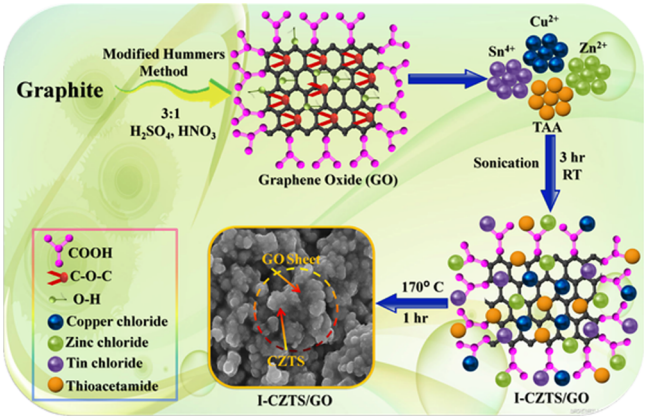

precursors and the role of GO as the support material which is further responsible for improving the HER activity (detailed synthesis steps are explained in more detail in the Experimental Section).

Figure 1a shows Fourier transform infrared (FTIR) spectra of GO, CZTS, and I-CZTS/GO over the range of 600−4000

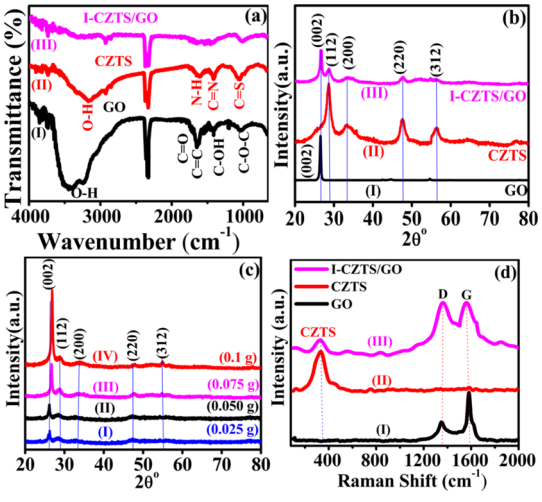

Figure 1. Superimposed (a) FTIR spectra of (I) GO (black), (II) CZTS (red), and (III) I-CZTS/GO composite (pink). (b) XRD pattern of (I) GO (black), (II) CZTS (red), and (III) I-CZTS/GO composite (pink). (c) XRD pattern with various amounts of GO loading in CZTS. (d) Raman spectra of (I) GO (black), (II) CZTS (red), and (III) I-CZTS/GO composite (pink).

cm^{-1}. The characteristic bands of GO are observed at 1025 cm^{-1} (C−O−C stretching of epoxy groups), 1406 cm^{-1} (C−OH stretching), 1615 cm^{-1} (C=C skeleton of graphitic domains), 1725 cm^{-1} (C=O stretching of COOH groups), and 3442 cm^{-1} (−O−H bending).[20] The intensities of these oxygen-containing functional groups decrease remarkably in the I-CZTS/GO composite sample, suggesting that GO is nearly reduced. The characteristic functional groups of CZTS were located in 1040, 1420, 1622, and 2351 cm^{-1}, corresponding to the C=S stretching, coupled vibrations of C=N stretching, N−H bending, and S−H thiol functionality, respectively, which are in agreement with the literature values.[21] On the other hand, the above assigned peaks were also observed in the I-CZTS/GO composites but with reduced intensity or disappearance, which indicates that the oxygenated functional groups in GO were reduced partially.

The phase purity and crystalline nature of the synthesized material have been confirmed by X-ray diffraction (XRD). Figure 1b shows the XRD patterns of GO, CZTS, and the I-CZTS/GO composite. The XRD pattern of GO portrays a distinct peak at (002), similar to few-layer graphene.[22] It is obvious that the XRD patterns of pure CZTS would show the characteristic peaks at (112), (200), (220), and (312) crystal planes of the kesterite structure of CZTS (JCPDS card no. 26-0575).[23] Moreover, the GO/CZTS nanocomposites possess the XRD pattern with the peaks observed at (002) (112), (200), (220), and (312), corresponding to the diffraction planes of mixed GO and CZTS. However, the composite shows peaks with lower intensities than those for pure CZTS. This is possible when graphene is wrapped around the surface of the CZTS particles,[24] which could further induce crystal diffraction. Figure 1c shows the XRD patterns of the CZTS/GO composite with varying amounts of GO loading in CZTS, that is, 0.025, 0.050, 0.075, and 0.1 g. It is observed that the peak intensity gradually increases with increasing GO loading, particularly for the (002) plane of GO. Similarly, four pronounced diffraction planes at (112), (200), (220), and (312) of CZTS were also observed. Raman spectra measurements were performed to obtain a more precise assignment of the structure of GO, CZTS, and CZTS/GO composites, and the results are shown in Figure 1d. The Raman profile of GO shows the presence of bands at 1355 and 1589 cm^{-1}, which correspond to D and G bands, respectively. The characteristic peak of CZTS at 333 cm^{-1} was assigned to the A1 mode, which is the strongest mode observed from kesterite CZTS. For the CZTS/GO composite, all the Raman bands for CZTS and GO were observed. Moreover, in the present study, the D and G bands for the CZTS/GO composite appeared at 1360 and 1594 cm^{-1}, respectively. When CZTS NPs are decorated on GO, the intensity of the D band is found to increase relative to the G band, and both the bands shift to higher wavenumbers could be due to their restrictive moments after CZTS deposition on graphene.[24] The XRD patterns accompanied with Raman spectra demonstrate the fact that the CZTS/GO composite material is obtained after the sonochemical process in this work.

Field emission scanning electron microscopy (FESEM) images in Figure 2a−d demonstrates the surface morphologies of GO sheets, pure CZTS, and I-CZTS/GO composite, respectively. From the FESEM image in Figure 2a, the layered structure of the stacked GO sheets is observed with wrinkles all over the surface of GO sheets.[25] The solid GO sample is severely agglomerated because of its high specific surface area. Figure 2b shows an FESEM image of pure CZTS, and it reveals that the morphology of CZTS is sphere-like and homogenously distributed with a narrow diameter of about 250−300 nm.[21a] As for the I-CZTS/GO nanocomposites shown in Figure 2c, it can be clearly observed that the CZTS spheres were well dispersed in the graphene framework with

DOI: 10.1021/acsomega.8b03587
ACS Omega 2019, 4, 7650−7657

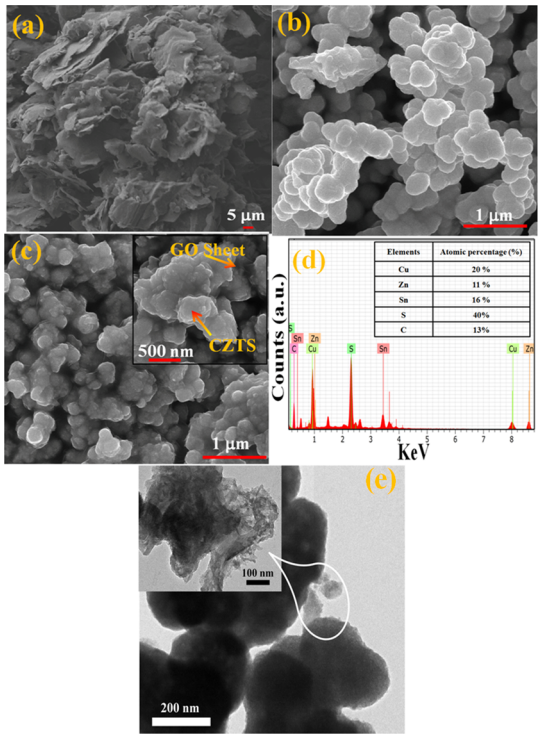

Figure 2. FESEM image of (a) GO, (b) pure CZTS, and (c) I-CZTS/GO composite and (inset 500 nm scale bar). (d) Energy-dispersive X-ray (EDX) spectrum of the I-CZTS/GO composite (e) TEM images of the I-CZTS/GO composite and the inset shows 100 nm scale bar.

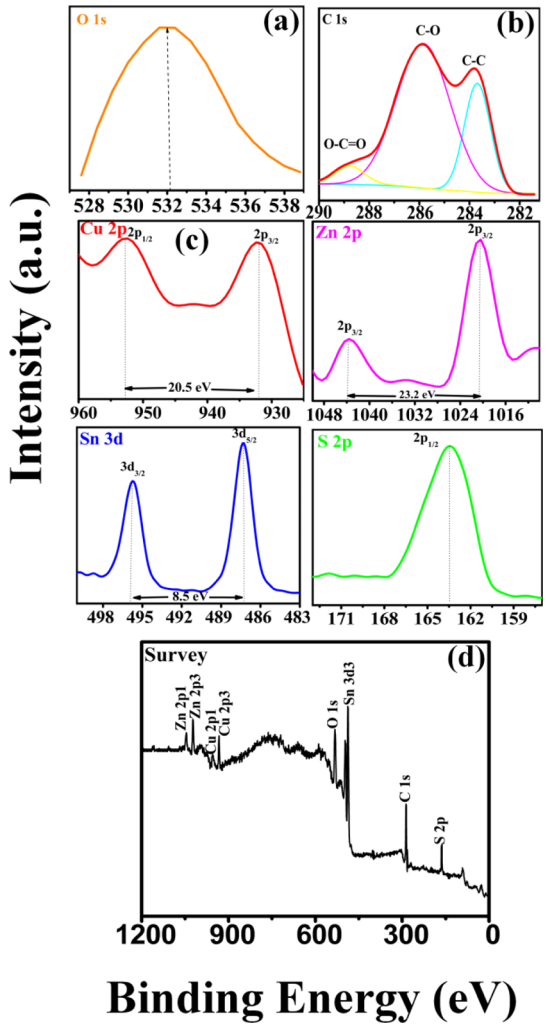

Figure 3. XPS of (a) oxygen (1s), (b) carbon (1s), (c) CZTS (Cu 2p, Zn 2p, Sn 3d, and S 2p), and (d) survey spectra of the I-CZTS/GO composite.

no obvious aggregation, and the majority of these CZTS spheres were wrapped with graphene nanosheets.[24] Further, to know the presence of CZTS on GO, the EDX spectrum was recorded for the I-CZTS/GO composites. The composition of the I-CZTS/GO composites is summarized with the recorded spectrum as shown in Figure 2d. The studies confirm that the presence of Cu, Zn, Sn, S, and carbon peaks represent the graphene.[26] Moreover, the transmission electron microscopy (TEM) image in Figure 2e clearly shows the CZTS particles wrapped in graphene sheets with a size of 225−300 nm, which is consistent with the observation from SEM images of CZTS/GO composites.

X-ray photoelectron spectroscopy (XPS) analyses (Figure 3) were performed to further investigate the surface composition and chemical states of the I-CZTS/GO composite.[27] Accordingly, the XPS survey spectrum shown in Figure 3d identifies the presence of Cu, Zn, Sn, S, and C in the CZTS/GO. The broad signal (Figure 3a) having binding energy from 520 to 540 eV corresponding to O 1s could be due to different oxygen containing functionalities available on GO. Moreover, Figure 3b C−O and C−C peaks appear with a strong signal and the O═C−O peak as a shoulder at 286.1, 283.8, and 288.5 eV, respectively.[28] Figure 3c shows two peaks at 933.9 and 953.7 eV in XPS spectra which were assigned to $2p_{3/2}$ and $2p_{1/2}$ with a splitting energy of 20.5 eV, corresponding to Cu(I). Moreover, the Zn(II) state was identified from the peaks at 1022.6 and 1044.5 eV with a splitting energy of 23.2 eV. The sharp Sn 3d peaks located at 486.6 and 495.1 eV with a peak separation of 8.5 eV confirmed the Sn(IV) state. The overlapping of sulfur $2p_{1/2}$ peaks were identified at 163.4 eV, which agreed with the sulfide phase in the range of 160 to 164 eV.[29] As can be seen from the XPS spectra, no other valences such as Cu(II) and Sn(II) were found corresponding to that of secondary phases CuS and Cu_2SnS_3. These XPS results are in good agreement with the reported literature.[23] The CZTS and I-CZTS/GO were further investigated by the Brunauer−Emmett−Teller (BET) method to calculate the specific surface area, and the nitrogen adsorption/desorption isotherms are shown in Figure S1. The CZTS exhibits a relatively low BET specific surface area of 2.016 m^2 g, whereas the surface area is higher (6.553 m^2 g) for the I-CZTS/GO composite because of the presence of graphene with the large surface area. The enhanced specific surface area provides efficient active sites and better transport pathways for charged ions, which is beneficial for the improvement of electrochemical performance of the composite. The Barrett−Joyner−Halenda pore size distribution indicates the high degree of uniformity of pores in the range of 3.578 nm for CZTS and 5.237 nm for I-CZTS/GO. Although the pore diameter for both samples is comparable, a larger pore diameter in I-CZTS/GO suggests more effective active sites leading to enhanced electrocatalytic activity. .It is in good agreement with the other findings from microscopy and spectroscopy data.

Electrocatalytic Performance toward HER. Electrocatalytic performance toward HER, of I-CZTS/GO compo-

DOI: 10.1021/acsomega.8b03587
ACS Omega 2019, 4, 7650−7657

sites, pure CZTS, and GO were examined using the three electrode system, where glassy carbon electrode (GCE), Pt foil, and saturated calomel electrode (SCE) are working, counter, and reference electrodes, respectively, in 0.5 M H_2SO_4 solution. Previous to linear sweep voltammetry (LSV) measurements, cyclic voltammetry (CV) was carried out to steady or drench the electrocatalysts in the electrolyte; the results are shown in Figure S2. Figure 4a superimposed LSV

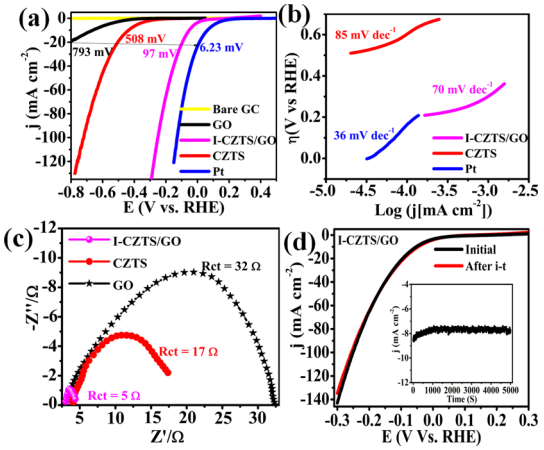

Figure 4. Superimposed (a) HER polarization curves of bare GC (yellow), GO (black), CZTS (red) I-CZTS/GO (pink), and Pt (blue), (b) corresponding to the Tafel plot of CZTS (red), I-CZTS/GO (pink), and Pt (blue). (c) Nyquist plot of the GO (black), CZTS (red), I-CZTS/GO (pink), and (d) the durability test of I-CZTS/GO in 0.5 M H_2SO_4 using Pt foil and SCE as a counter and reference electrode, respectively.

polarization curves of Pt, I-CZTS/GO composites, pure CZTS, and bare GO electrodes at a scan rate of 50 mV s^{-1}. As jurisdiction, the electrochemical performances for Pt and bare GCE electrodes were also examined for comparison and apparently, Pt demonstrates very small overpotential, indicating the superior electrocatalytic activity for HER,[32] while the bare GCE electrode shows very high overpotential confirming its negligible catalytic activity. I-CZTS/GO represents the overpotentials distinctly lower than CZTS.

Significantly, I-CZTS/GO shows an onset overpotential of 39.3 mV at 2 mA cm^{-2} and overpotentials of 53.1 and 97 mV to afford current densities of 10 and 20 mA cm^{-2}, respectively. The catalytic activity is higher than the former reported catalysts used in HER.[17a,30] Demonstrating the performances of CZTS and GO electrodes exhibits inferior HER activities as compared to I-CZTS/GO composites. The improved electrochemical performance of CZTS/GO composites can be credited to the electronic as well as chemical pairing between the CZTS and GO supporter[14,16] (see the schematic in Scheme 2).

Figure S4 demonstrates the comparison between I-CZTS/GO composites with varying amounts of GO loading, that is, 0.025, 0.050, 0.075, and 0.1 g. The GO synthesized CZTS/GO composite (0.075 g) shows a better result compared to all other loadings; hence, it is taken for all other studies. Figure 4b revealing the Tafel slope is the main index for evaluating HER performance, and a lower Tafel slope leads to a faster increment of the HER rate with rising overpotential. The linear portions of the Tafel plots were fitted by the Tafel equation ($\eta = b \log j + a$, where j is the current density and b is

Scheme 2. Schematic of HER on the I-CZTS/GO Composite

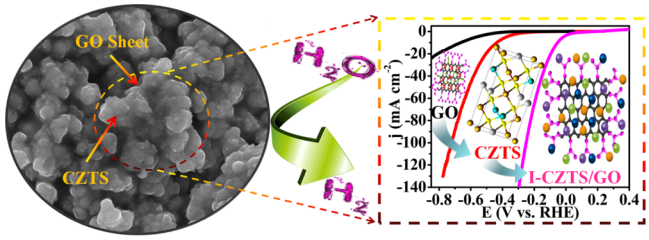

the Tafel slope), and I-CZTS/GO exhibits a Tafel slope of 70 mV dec^{-1} as shown in Figure 4b. The value is higher than 36 mV dec^{-1} for the Pt,[31] while it is much lower than 85 mV dec^{-1} for pure CZTS and moreover, most of the reported values for non-noble metal HER catalysts, such as MoS_2 alone,[32] MoS_2CFs,[33] bare CoS_2,[34] and other nonprecious metal catalysts are listed in (Table 1) The exchange current

Table 1. HER Activities of Nonprecious Metal Electrocatalysts from the Literature with Our Proposed System in the 0.5 M H_2SO_4 Electrolyte

sr. nos.	materials	overpotential (mV vs RHE) @ 10 mA cm^{-2}	Tafel slope (mV dec^{-1})	refs
1	pure MoS_2	520	78.2	35b
2	MoS_2 NS/CC	142	102.1	36
3	WS_2 NTs	400	121	37
4	Mn_3O_4	111	85	38
5	CoP	135	90	39
6	WSe_2−C-20	158	98	40
7	CoMox/CC	100	70	41
8	WS_2 powder	330	160	42
9	CoP nanorods	140	98	43
10	MoS_2/MoO_2	240	76.1	44
11	FeP NP	292	86	45
12	Co−B	250	75	46
13	Co−CZTS	298	73	47
14	Cu−MoS_2/rGO (12 wt %)	126	90	48
15	MoS_2 QDs/rGO	64	63	49
16	MoSSe@rGO	135	51	50
17	rGO/WS_2	229	73	48
18	Fe_2P@rGO	101	55.2	51
19	MoS_2AGs/rGO	290	102	16
20	**I-CZTS/GO**	**53.1**	**70**	**this work**

density (j_0) of the HER on I-CZTS/GO is obtained to be 908 mA cm^{-2}, higher than that of pure CZTS (882 mA cm^{-2}) and also outperforming many reported non-noble metal HER catalysts.[35] These results indicate the high catalytic activity of I-CZTS/GO with respect to most of the nonprecious systems from the literature. The LSV polarization curves of the I-CZTS/GO composite at various scan rates are shown in Figure S5, and it can be seen that the current density increases from 133 to 164 mA cm^{-2} with the rising scan rate from 10 to 100 mV s^{-1} at a potential of −0.3 V versus the reversible hydrogen electrode (RHE), showing that the catalytic activity of I-CZTS/GO composites toward HER is fewer pretentious by scan rates, which indicates interfacial electron transfer is diffusion controlled.[10] Electrochemical impedance spectroscopy (EIS) measurements were carried out to understand the

DOI: 10.1021/acsomega.8b03587
ACS Omega 2019, 4, 7650−7657

role of electrode kinetics and interface reaction of CZTS and its GO composites on HER.

Superimposed Nyquist plots for CZTS-based systems are shown in Figure 4c. The observed variable semicircles are because of having different charge transfer resistance (R_{ct}) capabilities at the electrified interface. Interestingly, from the data fitting, it has been confirmed that the I-CZTS/GO presents lower R_{ct} of (5 Ω) in comparison to CZTS (17 Ω), indicating enhancement in the electron transfer which goes to enhance HER from cooperative features with GO of CZTS.[52] Moreover, the catalytic stability of the I-CZTS/GO composite was also evaluated and is shown in Figure 4d. Accordingly, the LSV polarization curves of I-CZTS/GO demonstrating parallel polarization initially and after $i-t$ amperometry, revealing merely a negligible decrease of current density (∼9 mA cm^{-2}) and signifying that the I-CZTS/GO composite catalyst possesses superior long-standing constancy and is in good agreement with other electrochemical data and morphological studies. The catalyst contaminant from the electrode may contribute to the slight loss in catalytic activity.[35b,53] The inset of Figure 4d shows the performance of 5000 s of $i-t$ amperometry for stability test. Fascinatingly, morphological features of CZTS/GO by TEM after the $i-t$ measurements are shown in Figure S6, and no harsh corrosion was found even after a long-term operation of the potential in acidic medium at an applied potential. It signifies that the CZTS/GO is morphologically and structurally stable and having extraordinarily performance toward HER.

In real, the actual efficiency of the electrocatalytic systems were studied using the turnover frequency (TOF), which represents the number of hydrogen molecules produced per second per active site. TOF can be determined by BET surface area (6.553 m^2/g) of the I-CZTS/GO catalyst. The calculated TOF of H_2 molecules are 1.677 s^{-1} at η = 250 mV. (Details of calculations and comparison with the literature are given in Table S2 in the Supporting Information). Interestingly, to confirm further and support our justification about the HER response to I-CZTS/GO, the LSV polarization curve using graphite as the counter electrode instead of Pt (to further check the oxidation of counter electrode Pt and deposition of the working electrode) and found insignificant change in overpotential (Figure S3).

For supporting the observations, we employed the ex situ method for the synthesis of the CZTS/GO (E-CZTS/GO) composite using the facial sonochemical method as shown in the schematic (Scheme S1), and Figure S7a XRD pattern shows E-CZTS/GO. All the diffraction peaks in the XRD patterns of E-CZTS/GO are consistent with the tetragonal phase kesterite CZTS (JCPDS no 26-0575) and (002) plane reliable with GO Figure S7b. The Raman spectra of CZTS/GO composites showed G (1586 cm^{-1}) and D (1350 cm^{-1}) band structures of carbon, suggesting that the structure of graphene was maintained in the composites. The signal at 332.8 cm^{-1} could be assigned to the CZTS. Figure S8 shows morphology of E-CZTS/GO, and it is clearly seen that CZTS nanoparticles are distributed on GO, indicating that GO is giving support to CZTS and providing an efficient electrical network for electron transport during HER. Figure S9a−d shows that the E-CZTS/GO composite exhibited good catalytic activity for HER, and its scan rate-dependent polarization is shown in Figure S10. The overpotential of the composite was found to decrease from −0.8 mV of CZTS to −0.4 mV of the composite, with its low Tafel slope at 95 mV/dec, fast charge transfer resistance (12 Ω), and good stability after 1000 CV cycles, without any change in features of polarization curves. However, slight decay of current density is observed, indicating that the E-CZTS/GO composite catalyst retains excellent long-term stability.

CONCLUSIONS

In summary, CZTS was modified with GO by a simple sonochemical method; the GO does not influence the crystal phase of CZTS but makes it more dispersed. The I-CZTS/GO composite displays extraordinarily high electrocatalytic activity for hydrogen generation reaction, and the overpotential of this electrode is ∼39.3 mV with a Tafel slope of ∼70 mV/decade. Moreover, this electrode exhibits good stability with negligible current lost in the durability test. It is believed that the incorporation of graphene enhances the charge transfer abilities, improving the electrocatalytic H_2 evolution. The composite has lower resistance compared to GO in the all frequency region, demonstrating the faster transport of electrons for HER. The I-CZTS/GO composite possessed high electrocatalytic activity and excellent stability. Therefore, it could be a strong candidate of the HER catalyst.

EXPERIMENTAL SECTION

Chemicals and Materials. Graphite fine powder (extra pure), H_2SO_4, HNO_3, HCl, copper chloride, zinc chloride, tin chloride, thioacetamide, 2-methoxyethanol, monoethanolamine, and absolute ethanol of AR grade. All the chemicals were purchased from Sigma-Aldrich, and others were used without any further purification.

Preparation of GO. GO was synthesized according to the modified Hummers' method. In brief, 1 g of graphite powder was added in 3:1 H_2SO_4/HNO_3 under continuous stirring in ice bath for 30 min and further sonicated for 6 h at room temperature. The suspension was refluxed in an oil bath for 24 h. The mixture was then repeatedly centrifuged and washed in succession with water, 30% HCl solution, and deionized (DI) water.

Synthesis of CZTS Nanoparticles. CZTS nanoparticles were synthesized using the sonochemical method which is previously reported in our paper.[54] Briefly, for the preparation of sol Cu/Zn/Sn/TAA/monoethanolamine (MEA), (2:1:1:4:1) molar proportion was taken. Initially, 1 mol of $CuCl_2$ was liquefied in 100 mL of 2-methoxyethanol under stirring for 30 min followed by addition of 0.5 mol each of $SnCl_4$ and $ZnCl_2$ simultaneously into the solution followed by stirring for next 30 min to get clear precursor solution. Further, 2 mol thiol−alkane−amine (TAA) and a suitable quantity of monoethanolamine was added till the solution turned dark brown followed by sonication for next 1.5 h and the final black precipitate was obtained. This precipitate was then repeatedly washed by absolute ethanol to remove the unreacted reactant and other impurities and then annealed at 170 °C for 2 h.

Synthesis of in Situ CZTS/GO Composite. As-synthesized GO is dispersed in 100 mL of 2-methoxyethanol under vigorous stirring for 2 h to ensure good dispersion. The metal precursors, 1 M $CuCl_2$, 0.5 M $ZnCl_2$, and 0.5 M $SnCl_4$ were added in above solution with constant stirring for another 30 min to get a clear solution. To this solution, 2 M TAA and appropriate quantity of MEA was added under continuous stirring till the solution turned dark brown. This solution was then put into an ultrasonic bath for next 3 h to achieve the

DOI: 10.1021/acsomega.8b03587
ACS Omega 2019, 4, 7650−7657

black precipitate. The precipitate was repeatedly washed using absolute ethanol to remove the excess TAA and other physiadsorbed counter ions and then annealed at 170 °C (decomposition temperature) for 2 h.

Synthesis of Ex Situ CZTS/GO Composite. The synthesized CZTS (0.3 mg) was dispersed in 10 mL of 2-methoxyethanol. Then, 0.1 mg of GO and 0.4 mL of MEA was added to the above solution, and the mixture was stirred for 2 h and subsequently the precursor solution was put into an ultrasonic bath for 3 h at room temperature (RT). The final solution was filtered with an equal volume of ethanol. The obtained product was washed two times with ethanol and annealed at 170 °C for 1 h. These in situ and ex situ CZTS/GO were further characterized and used for electrocatalytic HER studies.

Material Characterizations. The product was analyzed by FTIR. The phase and structure were characterized using XRD (Siemens D-5005 diffractometer) equipped with an X-ray tube (Cu $K\alpha_1$; λ = 1.5418 nm, 40 kV, 30 mA, with a step size of 0.01°). FESEM and X-ray photoelectron spectroscopy (XPS) SPECS HSA-3500 with a monochromatic X-ray source of Al $K\alpha$ radiation and hemispherical analyzer were used to investigate the elemental states of the sample. Raman spectroscopy measurements were performed by Raman optics with the microscope, Seki Technotron Corp. Tokyo with a 532 nm laser. The electrochemical and electrocatalytic studies were performed using the three-electrode system with the electrochemical workstation (CHI-Instrument 660E, USA).

Electrochemical Measurements. The electrocatalytic HER performance of the above as-synthesized samples was tested by CV, LSV, and electrochemical impedance spectroscopy (EIS) analysis on an electrochemical workstation (CHI-660E) using a three-electrode system, a modified GCE (3 mm in dia.) as a working electrode, and SCE and Pt foil as the reference and counter electrodes, respectively. Prior to use, the GCE was polished by sequential use of 1, 0.3, and 0.05 μm alumina powders, followed by sonication in DI and methanol for 5 min each to remove inorganic and organic impurities. The working electrode was fabricated using 5.0 mg of the catalyst dispersed into a mixture of solvent containing 100:1 of isopropanol/Nafion (5 wt %) solution and then the mixture was sonicated for ∼30 min to form a homogeneous ink. Afterward, 10 μL (0.41 mg loading normalized to current density) of the catalytic ink was loaded onto the GCE and dried naturally at RT. CV and LSV were conducted in aqueous 0.5 M H_2SO_4 electrolytic solutions, and all the results were further reported with respect to RHE in 0.5 M H_2SO_4 E(RHE) = E(SCE) + 0.244 V. EIS measurements were carried out from 1 000 000 to 0.002 Hz.

■ ASSOCIATED CONTENT

Supporting Information

The Supporting Information is available free of charge on the ACS Publications website at DOI: 10.1021/acsomega.8b03587.

BET data, TEM after electrochemcial long term stability studies, CV and LSV with different scan rates, LSV polarization curve using the graphite electrode as a counter, LSV of different loading amounts, XRD, Raman, FESEM, and electrochemistry data of the E-CZTS/GO composite, schematic of E-CZTS/GO, electrochemical activity comparison with literature table, detailed calculation method to obtain the TOF value, and comparative table for TOF with literature (PDF).

■ AUTHOR INFORMATION

Corresponding Author

*E-mail: bhaskarsathe@gmail.com. Phone: +91-8275306471.

ORCID

Anil V. Ghule: 0000-0001-6295-0763

Bhaskar R. Sathe: 0000-0001-8989-0967

Notes

The authors declare no competing financial interest.

■ ACKNOWLEDGMENTS

Authors are thankful to DAE-BRNS, (F. no. 34/20/06/2014-BRNS/21gs) Mumbai (India), FAST-TRACK DST-SERB (F. no. SERB/F/7963/2014-15 and F. no. EMR/2016/003587) New Delhi (India) for financial support and Department of Chemistry, Dr. Babasaheb Ambedkar Marathwada University, Aurangabad for laboratory facilities. Author R.V.D. is thankful to DAE-BRNS for JRF fellowship.

■ REFERENCES

(1) (a) Winter, C.-J. Hydrogen energy - Abundant, efficient, clean: A debate over the energy-system-of-change☆. *Int. J. Hydrogen Energy* **2009**, *34*, S1−S52. (b) Ball, M.; Wietschel, M. The future of hydrogen - opportunities and challenges. *Int. J. Hydrogen Energy* **2009**, *34*, 615−627.

(2) Christopher, K.; Dimitrios, R. A review on exergy comparison of hydrogen production methods from renewable energy sources. *Energy Environ. Sci.* **2012**, *5*, 6640−6651.

(3) Raimondi, F.; Scherer, G. G.; Kötz, R.; Wokaun, A. Nanoparticles in energy technology: examples from electrochemistry and catalysis. *Angew. Chem.* **2005**, *44*, 2190−2209.

(4) (a) Ouyang, C.; Wang, X.; Wang, C.; Zhang, X.; Wu, J.; Ma, Z.; Dou, S.; Wang, S. Hierarchically porous Ni_3S_2 nanorod array foam as highly efficient electrocatalyst for hydrogen evolution reaction and oxygen evolution reaction. *Electrochim. Acta* **2015**, *174*, 297−301. (b) Zhang, A.; Yu, S.; Jiang, Y.; Jia, L.; Xia, X.; Ye, W.; Wang, C. A novel Pt@Te-reduced graphene oxide/polyimide composite catalyst for hydrogen evolution. *Int. J. Hydrogen Energy* **2015**, *40*, 16238−16247. (c) Zhu, L.; Cai, Q.; Liao, F.; Sheng, M.; Wu, B.; Shao, M. Ru-modified silicon nanowires as electrocatalysts for hydrogen evolution reaction. *Electrochem. Commun.* **2015**, *52*, 29−33.

(5) Cao, H.; Xie, Y.; Feng, Q.; Wang, H.; Wang, X.; Xu, Z.; Xiao, F.; Zhou, W.; Pan, K. Multifunctional catalysts with high catalytic activities: flower-like Co_9S_8 microballs assembled with weak crystalline pea pod-shaped nanowires. *Int. J. Hydrogen Energy* **2018**, *43*, 18832−18842.

(6) Gao, Y.; Lang, Z.; Yu, F.; Tan, H.; Yan, G.; Wang, Y.; Ma, Y.; Li, Y. A Co_2 P/WC nano-heterojunction covered with N-doped carbon as highly efficient electrocatalyst for hydrogen evolution reaction. *ChemSusChem* **2018**, *11*, 1082−1091.

(7) Guo, L.; Wang, J.; Teng, X.; Liu, Y.; He, X.; Chen, Z. A novel bimetallic NiMo carbide nanowire array for efficient hydrogen evolution. *ChemSusChem* **2018**, *11*, 2717.

(8) Wang, Y.; Zhang, B.; Pan, W.; Ma, H.; Zhang, J. 3 D Porous nickel-cobalt nitrides supported on nickel foam as efficient electrocatalysts for overall water splitting. *ChemSusChem* **2017**, *10*, 4170−4177.

(9) (a) Wen, Y.; Xia, Y.; Zhang, S. Tungsten disulphide nanorattle: A new type of high performance electrocatalyst for hydrogen evolution reaction. *J. Power Sources* **2016**, *307*, 593−598. (b) Harnisch, F.; Sievers, G.; Schröder, U. Tungsten carbide as electrocatalyst for

DOI: 10.1021/acsomega.8b03587
ACS Omega 2019, 4, 7650−7657

the hydrogen evolution reaction in pH neutral electrolyte solutions. *Appl. Catal., B* **2009**, *89*, 455−458.
(10) Ma, L.; Shen, X.; Zhou, H.; Zhu, G.; Ji, Z.; Chen, K. CoP nanoparticles deposited on reduced graphene oxide sheets as an active electrocatalyst for the hydrogen evolution reaction. *J. Mater. Chem. A* **2015**, *3*, 5337−5343.
(11) (a) Pan, Y.; Hu, W.; Liu, D.; Liu, Y.; Liu, C. Carbon nanotubes decorated with nickel phosphide nanoparticles as efficient nanohybrid electrocatalysts for the hydrogen evolution reaction. *J. Mater. Chem. A* **2015**, *3*, 13087−13094. (b) Zhang, X.; Shao, J.; Huang, W.; Dong, X. Three dimensional carbon substrate materials for electrolysis of water. *Sci. China Mater.* **2018**, *61*, 1143−1153. (c) Sick, T.; Hufnagel, A. G.; Kampmann, J.; Kondofersky, I.; Calik, M.; Rotter, J. M.; Evans, A.; Döblinger, M.; Herbert, S.; Peters, K.; Böhm, D.; Knochel, P.; Medina, D. D.; Fattakhova-Rohlfing, D.; Bein, T. Oriented films of conjugated 2D covalent organic frameworks as photocathodes for water splitting. *J. Am. Chem. Soc.* **2018**, *140*, 2085−2092. (d) Narwade, S. S.; Mulik, B. B.; Mali, S. M.; Sathe, B. R. Silver nanoparticles sensitized C $_{60}$ (Ag@C $_{60}$) as efficient electrocatalysts for hydrazine oxidation: Implication for hydrogen generation reaction. *Appl. Surf. Sci.* **2017**, *396*, 939−944.
(12) Liao, L.; Zhu, J.; Bian, X.; Zhu, L.; Scanlon, M. D.; Girault, H. H.; Liu, B. MoS_2 Formed on mesoporous graphene as a highly active catalyst for hydrogen evolution. *Adv. Funct. Mater.* **2013**, *23*, 5326−5333.
(13) Zhao, Y.; Xie, X.; Zhang, J.; Liu, H.; Ahn, H.-J.; Sun, K.; Wang, G. MoS_2 Nanosheets supported on 3D graphene aerogel as a highly efficient catalyst for hydrogen evolution. *Chem.—Eur. J.* **2015**, *21*, 15908.
(14) Niyitanga, T.; Kyung Jeong, H. Graphite oxide and molybdenum disulfide composite for hydrogen evolution reaction. *Chem. Phys. Lett.* **2017**, *685*, 451.
(15) Yin, X.; Sun, G.; Song, A.; Wang, L.; Wang, Y.; Dong, H.; Shao, G. A novel structure of Ni-(MoS_2/GO) composite coatings deposited on Ni foam under supergravity field as efficient hydrogen evolution reaction catalysts in alkaline solution. *Electrochim. Acta* **2017**, *249*, 52−63.
(16) Ma, C.-B.; Qi, X.; Chen, B.; Bao, S.; Yin, Z.; Wu, X.-J.; Luo, Z.; Wei, J.; Zhang, H.-L.; Zhang, H. MoS_2 nanoflower-decorated reduced graphene oxide paper for high-performance hydrogen evolution reaction. *Nanoscale* **2014**, *6*, 5624−5629.
(17) (a) Hou, Y.; Zhang, B.; Wen, Z.; Cui, S.; Guo, X.; He, Z.; Chen, J. A 3D hybrid of layered MoS_2/nitrogen-doped graphene nanosheet aerogels: an effective catalyst for hydrogen evolution in microbial electrolysis cells. *J. Mater. Chem. A* **2014**, *2*, 13795−13800.
(18) Duan, J.; Chen, S.; Chambers, B. A.; Andersson, G. G.; Qiao, S. Z. 3D WS_2 Nanolayers@Heteroatom-Doped Graphene Films as Hydrogen Evolution Catalyst Electrodes. *Adv. Mater.* **2015**, *27*, 4234−4241.
(19) Amin, B. G.; Swesi, A. T.; Masud, J.; Nath, M. $CoNi_2Se_4$ as an efficient bifunctional electrocatalyst for overall water splitting. *Chem. Commun.* **2017**, *53*, 5412−5415.
(20) (a) Cano, M.; Khan, U.; Sainsbury, T.; O'Neill, A.; Wang, Z.; McGovern, I. T.; Maser, W. K.; Benito, A. M.; Coleman, J. N. Improving the mechanical properties of graphene oxide based materials by covalent attachment of polymer chains. *Carbon* **2013**, *52*, 363−371. (b) Riaz, A.; Usman, A.; Hussain, Z. Synthesis of 4, 4′-stilbene dicarboxylic acid and aniline modified graphene oxide and its electrochemical performance for supercapacitors. *Int. J. Electrochem. Sci.* **2016**, *11*, 1099−1110.
(21) (a) Chaudhuri, T. K.; Tiwari, D. Earth-abundant non-toxic Cu_2ZnSnS_4 thin films by direct liquid coating from metal-thiourea precursor solution. *Sol. Energy Mater. Sol. Cells* **2012**, *101*, 46−50. (b) Patel, M.; Mukhopadhyay, I.; Ray, A. Structural, optical and electrical properties of spray-deposited CZTS thin films under a non-equilibrium growth condition. *J. Phys. D: Appl. Phys.* **2012**, *45*, 445103.
(22) (a) Sathe, B. R.; Zou, X.; Asefa, T. Metal-free B-doped graphene with efficient electrocatalytic activity for hydrogen evolution reaction. *Catal. Sci. Technol.* **2014**, *4*, 2023−2030. (b) Sapner, V. S.; Chavan, P. P.; Digraskar, R. V.; Narwade, S. S.; Mulik, B. B.; Mali, S. M.; Sathe, B. R. Tyramine functionalized graphene: metal-free electrochemical non-enzymatic biosensing of hydrogen peroxide. *ChemElectroChem* **2018**, *5*, 3191−3197.
(23) Wang, J.; Zhang, P.; Song, X.; Gao, L. Surfactant-free hydrothermal synthesis of Cu_2ZnSnS_4 (CZTS) nanocrystals with photocatalytic properties. *RSC Adv.* **2014**, *4*, 27805−27810.
(24) Ibrahim, I.; Lim, H. N.; Huang, N. M.; Pandikumar, A. Cadmium sulphide-reduced graphene oxide-modified photoelectrode-based photoelectrochemical sensing platform for copper(II) ions. *PLOS ONE* **2016**, *11*, No. e0154557.
(25) Li, B.; Liu, T.; Wang, Y.; Wang, Z. ZnO/graphene-oxide nanocomposite with remarkably enhanced visible-light-driven photocatalytic performance. *J. Colloid Interface Sci.* **2012**, *377*, 114−121.
(26) Ravula, S.; Zhang, C.; Essner, J. B.; Robertson, J. D.; Lin, J.; Baker, G. A. Ionic liquid-assisted synthesis of nanoscale $(MoS_2)_{(x)}(SnO_2)_{(1-x)}$, on reduced graphene oxide for the electrocatalytic hydrogen evolution reaction. *ACS Appl. Mater. Interfaces* **2017**, *9*, 8065−8074.
(27) Wang, X.; Xie, Y.; Bateer, B.; Pan, K.; Jiao, Y.; Xiong, N.; Wang, S.; Fu, H. Selenization of Cu_2ZnSnS_4 enhanced the performance of dye-sensitized solar cells: improved zinc-site catalytic activity for I_3^-. *ACS Appl. Mater. Interfaces* **2017**, *9*, 37662−37670.
(28) (a) Johra, F. T.; Lee, J.-W.; Jung, W.-G. Facile and safe graphene preparation on solution based platform. *J. Ind. Eng. Chem.* **2014**, *20*, 2883−2887. (b) Dong, Y.-l.; Zhang, X.-f.; Cheng, X.-l.; Xu, Y.-m.; Gao, S.; Zhao, H.; Huo, L.-h. Highly selective NO_2 sensor at room temperature based on nanocomposites of hierarchical nanosphere-like α-Fe2O3 and reduced graphene oxide. *RSC Adv.* **2014**, *4*, 57493−57500.
(29) Xie, W.; Jiang, X.; Zou, C.; Li, D.; Zhang, J.; Quan, J.; Shao, L. Synthesis of highly dispersed Cu_2ZnSnS_4 nanoparticles by solvothermal method for photovoltaic application. *Phys. E* **2012**, *45*, 16−20.
(30) Ma, L.; Shen, X.; Zhu, J.; Zhu, G.; Ji, Z. Co_3ZnC core-shell nanoparticle assembled microspheres/reduced graphene oxide as an advanced electrocatalyst for hydrogen evolution reaction in an acidic solution. *J. Mater. Chem. A* **2015**, *3*, 11066−11073.
(31) Bai, Y.; Zhang, H.; Li, X.; Liu, L.; Xu, H.; Qiu, H.; Wang, Y. Novel peapod-like Ni_2P nanoparticles with improved electrochemical properties for hydrogen evolution and lithium storage. *Nanoscale* **2015**, *7*, 1446−1453.
(32) Yan, Y.; Xia, B.; Qi, X.; Wang, H.; Xu, R.; Wang, J.-Y.; Zhang, H.; Wang, X. Nano-tungsten carbide decorated graphene as co-catalysts for enhanced hydrogen evolution on molybdenum disulfide. *Chem. Commun.* **2013**, *49*, 4884−4886.
(33) Hou, D.; Zhou, W.; Liu, X.; Zhou, K.; Xie, J.; Li, G.; Chen, S. Pt nanoparticles/MoS_2 nanosheets/carbon fibers as efficient catalyst for the hydrogen evolution reaction. *Electrochim. Acta* **2015**, *166*, 26−31.
(34) Peng, S. J.; Li, L. L.; Han, X. P.; Sun, W. P.; Srinivasan, M.; Mhaisalkar, S. G.; Cheng, F. Y.; Yan, Q. Y.; Chen, J.; Ramakrishna, S. Cobalt sulfide nanosheet/graphene/carbon nanotube nanocomposites as flexible electrodes for hydrogen evolution. *Angew. Chem.* **2014**, *126*, 12802−12807.
(35) (a) Liu, M.; Yang, L.; Liu, T.; Tang, Y.; Luo, S.; Liu, C.; Zeng, Y. Fe_2P/reduced graphene oxide/Fe_2P sandwich-structured nanowall arrays: a high-performance non-noble-metal electrocatalyst for hydrogen evolution. *J. Mater. Chem. A* **2017**, *5*, 8608−8615. (b) He, J. N.; Liang, Y. Q.; Mao, J.; Zhang, X. M.; Yang, X. J.; Cui, Z. D.; Zhu, S. L.; Li, Z. Y.; Li, B. B. 3D Tungsten-doped MoS_2 nanostructure: a low-cost, facile prepared catalyst for hydrogen evolution reaction. *J. Am. Chem. Soc.* **2016**, *163*, H299−H304. (c) Guo, K.; Li, W.; Zhang, J.; Zhang, X.; Wang, X.; Chen, G.; Xu, T.; Yang, L.; Zhu, W.; Wei, B. Extremely high external quantum efficiency of inverted organic light-emitting diodes with low operation voltage and reduced efficiency roll-off by using sulfide-based double electron injection layers. *RSC Adv.* **2016**, *6*, 55626−55634.
(36) Zhu, W.; Tang, C.; Liu, D.; Wang, J.; Asiri, A. M.; Sun, X. A self-standing nanoporous MoP_2 nanosheet array: an advanced pH-

DOI: 10.1021/acsomega.8b03587
ACS Omega 2019, 4, 7650−7657

universal catalytic electrode for the hydrogen evolution reaction. *J. Mater. Chem. A* **2016**, *4*, 7169−7173.
(37) Seo, B.; Jeong, H. Y.; Hong, S. Y.; Zak, A.; Joo, S. H. Impact of a conductive oxide core in tungsten sulfide-based nanostructures on the hydrogen evolution reaction. *Chem. Commun.* **2015**, *51*, 8334−8337.
(38) Ray, C.; Dutta, S.; Negishi, Y.; Pal, T. A new stable Pd-Mn_3O_4 nanocomposite as an efficient electrocatalyst for the hydrogen evolution reaction. *Chem. Commun.* **2016**, *52*, 6095−6098.
(39) Pan, Y.; Lin, Y.; Chen, Y.; Liu, Y.; Liu, C. Cobalt phosphide-based electrocatalysts: synthesis and phase catalytic activity comparison for hydrogen evolution. *J. Mater. Chem. A* **2016**, *4*, 4745−4754.
(40) Zou, M.; Chen, J.; Xiao, L.; Zhu, H.; Yang, T.; Zhang, M.; Du, M. WSe_2 and $W(Se_xS_{1-x})_2$ nanoflakes grown on carbon nanofibers for the electrocatalytic hydrogen evolution reaction. *J. Mater. Chem. A* **2015**, *3*, 18090−18097.
(41) Zhang, N.; Ma, W.; Jia, F.; Wu, T.; Han, D.; Niu, L. Controlled electrodeposition of $CoMoS_x$ on carbon cloth: A 3D cathode for highly-efficient electrocatalytic hydrogen evolution. *Int. J. Hydrogen Energy* **2016**, *41*, 3811−3819.
(42) Yu, S.; Kim, J.; Yoon, K. R.; Jung, J.-W.; Oh, J.; Kim, I.-D. Rational design of efficient electrocatalysts for hydrogen evolution reaction: single layers of WS_2 nanoplates anchored to hollow nitrogen-doped carbon nanofibers. *ACS Appl. Mater. Interfaces* **2015**, *7*, 28116−28121.
(43) Wang, C.; Jiang, J.; Zhou, X.; Wang, W.; Zuo, J.; Yang, Q. Alternative synthesis of cobalt monophosphide@C core-shell nanocables for electrochemical hydrogen production. *J. Power Sources* **2015**, *286*, 464−469.
(44) Yang, L.; Zhou, W.; Hou, D.; Zhou, K.; Li, G.; Tang, Z.; Li, L.; Chen, S. Porous metallic MoO_2-supported MoS_2 nanosheets for enhanced electrocatalytic activity in the hydrogen evolution reaction. *Nanoscale* **2015**, *7*, 5203−5208.
(45) Liu, Q.; Pu, Z.; Asiri, A. M.; Sun, X. Nitrogen-doped carbon nanotube supported iron phosphide nanocomposites for highly active electrocatalysis of the hydrogen evolution reaction. *Electrochim. Acta* **2014**, *149*, 324−329.
(46) Gupta, S.; Patel, N.; Miotello, A.; Kothari, D. C. Cobalt-boride: an efficient and robust electrocatalyst for hydrogen evolution reaction. *J. Power Sources* **2015**, *279*, 620−625.
(47) Digraskar, R. V.; Sapner, V. S.; Narwade, S. S.; Mali, S. M.; Ghule, A. V.; Sathe, B. R. Enhanced electrocatalytic hydrogen generation from water via cobalt-doped Cu_2ZnSnS_4 nanoparticles. *RSC Adv.* **2018**, *8*, 20341−20346.
(48) Shifa, T. A.; Wang, F.; Cheng, Z.; Zhan, X.; Wang, Z.; Liu, K.; Safdar, M.; Sun, L.; He, J. A vertical-oriented WS_2 nanosheet sensitized by graphene: an advanced electrocatalyst for hydrogen evolution reaction. *Nanoscale* **2015**, *7*, 14760−14765.
(49) Li, F.; Li, J.; Cao, Z.; Lin, X.; Li, X.; Fang, Y.; An, X.; Fu, Y.; Jin, J.; Li, R. MoS_2 quantum dot decorated RGO: a designed electrocatalyst with high active site density for the hydrogen evolution reaction. *J. Mater. Chem. A* **2015**, *3*, 21772−21778.
(50) Konkena, B.; Masa, J.; Xia, W.; Muhler, M.; Schuhmann, W. MoSSe@reduced graphene oxide nanocomposite heterostructures as efficient and stable electrocatalysts for the hydrogen evolution reaction. *Nano Energy* **2016**, *29*, 46−53.
(51) Liu, M.; Yang, L.; Liu, T.; Tang, Y.; Luo, S.; Liu, C.; Zeng, Y. Fe_2P/reduced graphene oxide/Fe_2P sandwich-structured nanowall arrays: a high-performance non-noble-metal electrocatalyst for hydrogen evolution. *J. Mater. Chem. A* **2017**, *5*, 8608−8615.
(52) (a) Kamila, S.; Mohanty, B.; Samantara, A. K.; Guha, P.; Ghosh, A.; Jena, B.; Satyam, P. V.; Mishra, B.; Jena, B. K. Highly active 2D layered MoS_2-rGO hybrids for energy conversion and storage applications. *Sci. Rep.* **2017**, *7*, 8378. (b) Zhang, J.; Zhao, L.; Liu, A.; Li, X.; Wu, H.; Lu, C. Three-dimensional MoS_2/rGO hydrogel with extremely high double-layer capacitance as active catalyst for hydrogen evolution reaction. *Electrochim. Acta* **2015**, *182*, 652−658.
(53) (a) Popczun, E. J.; Read, C. G.; Roske, C. W.; Lewis, N. S.; Schaak, R. E. Highly active electrocatalysis of the hydrogen evolution reaction by cobalt phosphide nanoparticles. *Angew. Chem.* **2014**, *126*, 5531−5534. (b) Kush, P.; Deori, K.; Kumar, A.; Deka, S. Efficient hydrogen/oxygen evolution and photocatalytic dye degradation and reduction of aqueous Cr(VI) by surfactant free hydrophilic Cu_2ZnSnS_4 nanoparticles. *J. Mater. Chem. A* **2015**, *3*, 8098−8106.
(54) Digraskar, R. V.; Mulik, B. B.; Walke, P. S.; Ghule, A. V.; Sathe, B. R. Enhanced Hydrogen Evolution Reactions on Nanostructured Cu_2ZnSnS_4 (CZTS) Electrocatalyst. *Appl. Surf. Sci.* **2017**, *412*, 475−481.

DOI: 10.1021/acsomega.8b03587
ACS Omega 2019, 4, 7650−7657